Estuarine Adjustment

Dependence of Salinity Delay on the Forcing Timescale and Magnitude

Dijkstra, Yoeri M.

DOI
10.1029/2023JC020162

Publication date
2024

Document Version
Final published version

Published in
Journal of Geophysical Research: Oceans

JGR Oceans

RESEARCH ARTICLE
10.1029/2023JC020162

Special Collection:
Physical processes, sediment transport and morphodynamics of estuaries and coastal seas

Estuarine Adjustment: Dependence of Salinity Delay on the Forcing Timescale and Magnitude

Yoeri M. Dijkstra[1]

[1]Delft Institute of Applied Mathematics, Delft University of Technology, Delft, The Netherlands

Abstract The salinity in estuaries continuously adapts to varying forcing for example, by discharge and tidal conditions. The changes in salinity lag behind the changes in forcing. Previous work has mostly related this delay to the *adjustment time*, which depends on an average background state of the estuary. Payo-Payo et al. (2022), https://doi.org/10.1029/2021jc017523 showed that adjustment time however cannot explain the actually observed delays for a realistic salinity and forcing signal. Inspired by this, this study aims to develop relations between delay time and forcing variations and background state of the estuary. To this end, I first propose a definition of the actual delay of salinity based on wavelet analysis, applicable to observed or modeled salinity signals. To compare delay to estuarine parameters, I use a linear 1D model, but qualitative results carry over to the general case. Using model experiments with harmonic and peaked variations in the forcing, the delay time depends not only on the adjustment time, but also on the timescale of the forcing variation. Even for forcing timescales that are up to a factor 100 longer than the adjustment time, both forcing timescale and adjustment time are important for the delay. A second novel finding is that the delay depends strongly on the position along the estuary where the delay is observed. As verification, model experiments with realistically varying forcing were done, roughly inspired by the Modaomen Estuary (China). Although delay times showed a complicated and scattered dependency on model variables in this case, the above qualitative conclusions were confirmed.

Plain Language Summary The salinity in estuaries continuously changes with changes in external conditions including river flow and tides. These changes of salinity lag behind the changes in external conditions. Previous work has mostly related this delay to a theoretical indicator, the adjustment time, that is related to a background state of the estuary. The adjustment time is useful as it is easy to compute and intuitive. However, recent research could not identify a clear relation between the actual delay and the adjustment time. Inspired by this, this study aims to develop relations between the delay time and the background state of the estuary. This was done using a simplified model. It was found that the delay time depends not only on the adjustment time, but also on the timescale and magnitude of variations of the external conditions. A second novel finding is that the delay depends strongly on the position along the estuary where the delay is observed, where locations further upstream experience a much longer delay between salinity and variations of external conditions. To verify these results, model experiments with realistically varying forcing were done, roughly inspired by the Modaomen Estuary (China).

Key Points:

- A new wavelet-based definition for delay of salinity to forcing was developed, potentially applicable to any observed or modeled salinity
- The delay time does not only depend on the background state of the estuary but also strongly on the timescale of changes in forcing
- Delay depends on the position along the estuary, with low-salinity areas experiencing longer delays than high-salinity areas

Supporting Information:

Supporting Information may be found in the online version of this article.

Correspondence to:

Y. M. Dijkstra,
y.m.dijkstra@tudelft.nl

Citation:

Dijkstra, Y. M. (2024). Estuarine adjustment: Dependence of salinity delay on the forcing timescale and magnitude. *Journal of Geophysical Research: Oceans*, *129*, e2023JC020162. https://doi.org/10.1029/2023JC020162

Received 22 JUN 2023
Accepted 12 APR 2024

Author Contribution:

Conceptualization: Yoeri M. Dijkstra
Formal analysis: Yoeri M. Dijkstra
Investigation: Yoeri M. Dijkstra
Methodology: Yoeri M. Dijkstra
Software: Yoeri M. Dijkstra
Validation: Yoeri M. Dijkstra
Visualization: Yoeri M. Dijkstra
Writing – original draft: Yoeri M. Dijkstra

1. Introduction

Estuaries are subject to continuously changing flow on multiple time scales due to varying tidal forcing and river run-off. The time scales include the tidal time scale (hours), river discharge events (days), spring-neap cycle (14 days) and seasonal river discharge variations (months). The salinity distribution in estuaries adjusts to these changing flow conditions with a certain delay (e.g., Banas et al., 2004; Gong & Shen, 2011). This delay may be anywhere from a few hours to months (e.g., Kranenburg, 1986; Vijith et al., 2009) depending on the estuary and the flow conditions. It is important to know how this delay depends on the estuary and the flow conditions to understand when critical salt intrusion may occur, leading to disruptions in use of fresh water for irrigation or consumption. Hence, this is important knowledge for developing effective management of estuaries.

Our main understanding of delayed salinity response today comes from both analytical and numerical model studies that consider idealized model experiments. Kranenburg (1986) and MacCready (1999); MacCready (2007) considered the "step experiment": simulating a sudden increase in discharge ΔQ starting from equilibrium conditions. If ΔQ is small compared to the background discharge Q_0, they found that the salinity adapts like a relaxation process with an exponential adjustment time scale T_{adj} that scales as

$$T_{\text{adj}} \sim \frac{AL_0}{Q_0}. \quad (1)$$

Here A is the cross-sectional area and L_0 an equilibrium salt intrusion length scale. MacCready (1999) noted that T_{adj} is smaller than the above expression for large positive ΔQ (i.e., as Q increases), while Hetland and Geyer (2004) found that T_{adj} is larger for large negative ΔQ (i.e., as Q decreases). Chen (2015) provides improved expressions for T_{adj} that capture this asymmetry.

Considering periodic variations of tidal dispersion, Hetland and Geyer (2004) and Lerczak et al. (2009) showed that the delay of salinity variations was not necessarily related to T_{adj}. If the period of the variations in tidal dispersion is small compared to T_{adj}, the delay in salinity response is 25% of this period, and hence much smaller than T_{adj}. Studying a single (positive) peak in river discharge, Monismith (2017) studied the delay in terms of relaxation. He found that the delay in salinity response depends on the duration of the peak, with longer peaks resulting in a longer relaxation times. Other authors also studied estuarine adjustment to periodic variations (Bowen & Geyer, 2003; Lerczak et al., 2009; MacCready, 2007) or single peaks (Biemond et al., 2022; Monismith, 2017), but focussed on the magnitude of the salinity response, not the delay. These studies showed that the magnitude of the salinity response decreases strongly if the period or peak duration is small compared to T_{adj}.

Recently, analyzing 9 months of realistic 3D model results of the Modaomen estuary (China) using wavelet transforms, Payo-Payo et al. (2022) (*hereafter* PP22) suggested that the delay in response of the salinity depends in a complex way on the typical time scale with which the forcing (e.g., tide or river discharge) varies and on the background (i.e., time-averaged) state of tidal amplitude, discharge and salinity in the estuary. For example, during the dry season they estimated a delay time of the salinity of about 1–3 hr with respect to M_2 tidal variations, 1 day with respect to short river discharge events, and several days with respect to slower variations in discharge and the spring-neap cycle. Much shorter delays were observed during the wet season. The observed seasonal trends in the delay time are consistent with expression 1. Also, the dependence of the delay on the forcing time scale is qualitatively consistent with the conclusions from the idealized experiments of Hetland and Geyer (2004), Lerczak et al. (2009) and Monismith (2017), that is, forcing variations on shorter time scales generally correlate with shorter delays. However, PP22 could not directly link their observed delay times to estimates involving T_{adj} suggested by previous authors. Hence, the delays observed in realistic model output remain largely unexplained. This is because we lack an overarching theory that connects the observed delay to T_{adj} and the forcing time scale at the same time.

In view of this, the goal of this work is to describe the delay of changes in salinity to changes in forcing (here focusing on dispersion, e.g. by the tide, and river discharge) as a function of the time scale and magnitude of these changes in forcing and of the background state of the estuary. To this end I first develop a definition of delay time based on wavelet analysis. This delay time can be computed for any measured or modeled salinity signal in a fully automated way and is hence general and objective. Next, I focus is on describing the qualitative behavior of the delay in a systematic way and covering a large range of parameters representative for many estuaries. Hence, I use a simple linear 1D salinity model, which is simple enough to analyze in detail. I will argue in Section 4 that the main results qualitatively carry over to nonlinear models. The main results and dependencies will be inferred from model experiments with idealized periodic variations and peaks in forcing. The model is then applied to a realistic forcing inspired by PP22 to test to what extent these theoretical results can be applied in realistic applications.

Section 2 presents the model, the parameters that control the model behavior, the solution method, and the analysis method using wavelet transforms. Notably, Section 2.5 provides the definition for delay time based on wavelet analysis. Next, Section 3 shows the resulting salinity delay in response to periodic forcing and peak variations in forcing. Section 4 presents a reflection on the theoretical results by applying the model to a realistic and complex forcing signal and by discussing to what extent the results can be transferred to more realistic nonlinear models. Finally, Section 5 summarizes the main conclusions.

2. Model and Methods

2.1. Linear Salinity Model

I consider a cross-sectionally averaged model for an estuary. The cross-sectional area is denoted by A and is assumed constant in the along-channel x-direction. The x-coordinate is positive in upstream direction, where $x = 0$ denotes the mouth. The water motion consists of a river discharge $Q(t)$, where t denotes time. The tidal flow, vertical and lateral exchange flows and wind are not resolved explicitly, but their effect on the salt distribution is parametrized by a dispersion parameter $K_h(t)$. Even though in practice, parametrizations of K_h depends in complex way on the flow and salinity itself, in the remainder of this study it will be referred to as a forcing parameter.

To describe the salt distribution $s(x, t)$, I use a linearized cross-sectionally integrated mass balance

$$As_t - Qs_x - AK_h s_{xx} = 0, \qquad (x > 0,\ t > 0). \tag{2}$$

Here, subscripts x, t denote derivatives with respect to these dimensions. At the mouth, the salinity is assumed to be known and equal to $s(0, t) = s_{\text{sea}}(t)$. For $x \to \infty$ the salinity is assumed to vanish. This salinity model has three forcing parameters: the discharge $Q(t)$, dispersion parameter $K_h(t)$ and boundary salinity $s_{\text{sea}}(t)$. Various time signals for these three parameters will be considered: harmonic functions, single peaks, and a realistic 9-month data set derived from 3D model results and observations.

2.2. Typical Length and Time Scales

To facilitate systematic analysis of the model it is useful to derive typical length and time scales present in Equation 2. To this end, I define the following scales: $s = s_{\text{sea},0}s^*$, $Q = Q_0Q^*$, $K_h = K_{h,0}K_h^*$, $t = T_{\text{adj},0}t^*$, $x = L_0x^*$. Here, variables with * denote dimensionless quantities, $s_{\text{sea},0}$, Q_0, and $K_{h,0}$ are typical scales for the forcing parameters, $T_{\text{adj},0}$ is a typical adjustment time scale, and L_0 is a typical salt intrusion length scale. Note that the scales Q_0 and $K_{h,0}$ are allowed to vary (gradually) with time. Substituting these expressions in Equation 2 and rewriting yields

$$s^*_{t^*} - \frac{T_{\text{adj},0}Q_0}{AL_0}Q^*s^*_{x^*} - \frac{T_{\text{adj},0}K_{h,0}}{L_0^2}K_h^*s^*_{x^*x^*} = 0.$$

Assuming all three terms in the equation are of a similar order of magnitude, it follows that $\frac{T_{\text{adj},0}Q_0}{AL_0}$ and $\frac{T_{\text{adj},0}K_{h,0}}{AL_0}$ are both equal to one. The expressions for $T_{\text{adj},0}$ and L_0 to satisfy these conditions are given by

$$L_0 = \frac{AK_{h,0}}{Q_0}, \tag{3}$$

$$T_{\text{adj},0} = \frac{AL_0}{Q_0}, \tag{4}$$

$$= \frac{A^2K_{h,0}}{Q_0^2}. \tag{5}$$

This expression for $T_{\text{adj},0}$ matches definitions in literature for T_{adj} (see Equation 1) up to a constant of proportionality and noting that various authors employed various definitions for L_0 (e.g., compare MacCready (2007, Equation 4.6), Monismith (2017, Equation 12), Lerczak et al. (2009, Equation 9)).

2.3. Solution Method

The solution method used depends on the type of forcing signal. For a purely harmonic forcing signal, two different analytical approximation solutions are used depending on the amplitude of the harmonic forcing. For the case of peak forcing or a general forcing signal, a numerical discretization is used. The solution methods are briefly discussed below, with more details in SI-1.

Small-amplitude harmonic forcing: I first consider the case of small-amplitude harmonic forcing. Of the three forcings in the model, Q, K_h, and s_{sea} I only vary one at a time, keeping the others constants. These forcing variations have the form.

$$Q = Q_0 + \Re\left(\hat{Q}_1 e^{-i2\pi\frac{t}{T_{\text{forcing}}}}\right), \text{ or} \tag{6a}$$

$$K_h = K_{h,0} + \Re\left(\hat{K}_{h,1} e^{-i2\pi\frac{t}{T_{\text{forcing}}}}\right), \text{ or} \tag{6b}$$

$$s_{\text{sea}} = s_{\text{sea},0} + \Re\left(\hat{s}_{\text{sea},1} e^{-i2\pi\frac{t}{T_{\text{forcing}}}}\right). \tag{6c}$$

Here, T_{forcing} is the period of the forcing signal, which will be varied in the model experiments. $\hat{Q}_1$ denotes a complex phase-amplitude with $\frac{|\hat{Q}_1|}{Q_0} \ll 1$, and similar notation is used for the other forcing parameters. The solution for s is constructed by using a perturbation expansion (see SI for details). The resulting salinity consists of a constant $s_0(x)$ plus small harmonic variation, that is,

$$s(x,t) = s_0(x) + \Re\left(\hat{s}_1(x) e^{-i2\pi\frac{t}{T_{\text{forcing}}}}\right), \tag{7}$$

where $\hat{s}(x)$ is the complex phase-amplitude also with $\frac{|\hat{s}|}{s_0} \ll 1$ everywhere. The solutions for s_0 and $\hat{s}_1$ can be found explicitly and read as

$$s_0(x) = s_{\text{sea},0} e^{-\frac{x}{L_0}}, \tag{8}$$

$$\hat{s}_1(x) = \begin{cases} -s_{\text{sea},0}\frac{i}{2\pi}\frac{T_{\text{forcing}}}{T_{\text{adj},0}}\frac{\hat{Q}^1}{Q_0} e^{-\frac{x}{L_0}}\left(1 - e^{-\frac{x}{2L_0}\left(\sqrt{1-8\pi i\frac{T_{\text{adj},0}}{T_{\text{forcing}}}}-1\right)}\right) & \text{if } \hat{K}_h \neq 0, \\ s_{\text{sea},0}\frac{i}{2\pi}\frac{T_{\text{forcing}}}{T_{\text{adj},0}}\frac{\hat{K}_{h,1}}{K_{h,0}} e^{-\frac{x}{L_0}}\left(1 - e^{-\frac{x}{2L_0}\left(\sqrt{1-8\pi i\frac{T_{\text{adj},0}}{T_{\text{forcing}}}}-1\right)}\right) & \text{if } \hat{Q} \neq 0, \\ \hat{s}_{\text{sea},1} e^{-\frac{x}{2L_0}\left(1+\sqrt{1-8\pi i\frac{T_{\text{adj},0}}{T_{\text{forcing}}}}\right)} & \text{if } \hat{s}_{\text{sea}} \neq 0. \end{cases} \tag{9}$$

General-amplitude harmonic forcing: if the forcing is harmonic with general amplitude, the forcing 6a–6c is still used but without restrictions on the amplitude of the harmonic part. The solution s then no longer consists just the single harmonic with period T_{forcing} but also of all multiples of this frequency. This is written as

$$s(x,t) = s_0(x) + \sum_{n=1}^{N} \Re\left(\hat{s}_n(x) e^{-ni\frac{2\pi t}{T_{\text{forcing}}}}\right). \tag{10}$$

Here, $N \to \infty$ yields the exact solution, but good approximations are achieved for finite N. Fixing $N = 30$ and substituting the above form for s and expressions 6a–6c in the model equation, analytical solutions can be computed. However, the resulting expressions are very long and complicated and therefore only evaluated numerically. The solution procedure is explained in the SI.

General forcing: for all other forms of the forcing terms, a numerical solution is used. To this end, the equation is discretized using a backward Euler method in time. The spatial discretization uses a first-order upwind method for advective terms and a second-order central method for dispersive terms. The length of the domain is chosen much longer than the salt intrusion length. The grid is equidistant.

2.4. Wavelet Analysis

Following Payo-Payo et al. (2022) results are analyzed using a wavelet transform. The wavelet transform provides a way of analyzing any signal consisting of temporal variations on multiple timescales and is therefore a useful and universal analysis tool for estuaries (e.g., Hoitink & Jay, 2016). The reader is referred to Grinsted et al. (2004) and Torrence and Compo (1998) for an extensive explanation of wavelet analysis. A brief summary is given below.

I use the Morlet$_{\omega 0=6}$ wavelet, which is a Fourier mode multiplied by a Gaussian function. The resulting transform acts like a Fourier transform, but on a Gaussian time window centered at time t. The size of this Gaussian window scales with the Fourier period T_{forcing}. Hence, the window is small when extracting high-frequency modes from the signal, while it is larger when extracting lower-frequency modes. Various wavelet transforms may be computed using this wavelet. First, the Continuous Wavelet Transform (CWT) computes the power of a signal (i.e., forcing or salinity) as a function of Fourier period T_{forcing} and window position t. Second, the Cross-Wavelet Transform (XWT) computes the common power of one forcing parameter and the salinity together as a function of T_{forcing} and t. Finally, the Cross-Wavelet Coherence (WCT) is like the XWT but normalized by the CWT of the forcing and salinity. The WCT is therefore like a correlation coefficient in the (t, T_{forcing})-space.

Of greatest relevance to this study, the WCT not only computes the correlation amplitude but also the phase difference $\phi(t, T_{\text{forcing}})$ between the forcing and salinity as a function of t and T_{forcing}. This phase difference provides information on the time delay (a precise definition is provided in the next section). A major advantage of wavelets over some other transforms, such as the Fourier transform, is the ability to identify changes in delay at each certain timescale over time. Hence, it is possible to identify that the delay between salinity and discharge on a weekly scale is different during the high and low discharge season. Fourier transforms on the other hand would only yield one value of the delay at each timescale.

For this study, I consistently used 146 wavelets with a period between 2 hr and 1 year (log-scale). Since the Morlet wavelets are non-orthogonal, adding wavelets could lead to different results in case of too low resolution. It was tested here that adding more wavelets to the analysis did not visibly alter the results.

2.5. Definitions of Delay and Adjustment Time

To formally define the delay time, let $\phi(t, T_{\text{forcing}})$ be the phase difference resulting from the cross-wavelet coherence. The delay time is given by

$$T_{\text{delay}}\left(t, T_{\text{forcing}}\right) = \begin{cases} \dfrac{\phi\left(t, T_{\text{forcing}}\right)}{2\pi} T_{\text{forcing}} & \text{for forcing } K_h \text{ and } s_{\text{sea}}, \\ \dfrac{\phi\left(t, T_{\text{forcing}}\right) + \pi}{2\pi} T_{\text{forcing}} & \text{for forcing } Q. \end{cases} \tag{11}$$

When considering forcing by Q the phase difference is shifted by π (i.e., 180°) as increasing Q leads to decreasing salinity, which is retrieved as a 180° phase difference. The delay time as defined here is the *actually observed delay time* between a certain (time-dependent) frequency in forcing and salinity. The above definition can be applied to any measured or modeled signal and will be used consistently throughout this study.

The value of T_{delay} is not meaningful for all t and T_{forcing}. If the forcing or salinity have almost no power at a certain forcing period and time, the delay is still defined but carries little significance. Hence, I only consider the time delay at points in the (t, T_{forcing})-space where the XWT and WCT are both significant and where the CWT of the forcing has a local maximum in T_{forcing}. To illustrate this procedure, consider some forcing varying at both a 7-day and 14-day scale but with noise as shown in Figure 1a. Figure 1b shows a colormap of the normalized CWT of the forcing as a function of time and wavelet scale, with warmer colors indicating more power. This shows power mainly in the area around the 7 and 14 days wavelet scales. The red lines show the significance thresholds for the XWT compared to a red noise model with 95% confidence level. This shows only significant results roughly within the 5–19 days band. The WCT is significant in the entire domain in this simple case and is hence not shown. Within the area where the XWT and WCT are significant, only the forcing bands where the CWT attains local maxima are selected and indicated by the black markings. These clearly are at the 7 and 14 days wavelet timescales with a few spurious points due to the noise.

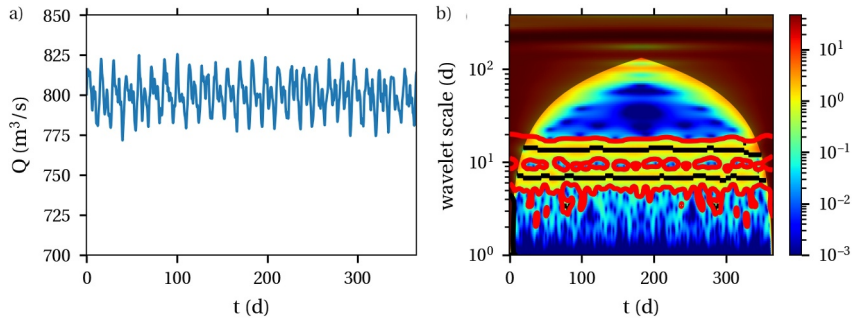

Figure 1. Illustration of use of wavelets to select the relevant timescales to compute delay. (a) illustration of a forcing with a 7 and 14 days forcing and noise. (b) normalized Continuous Wavelet Transform of the forcing (colors), significance threshold of the Cross-Wavelet Transform (red lines) and selected points for analysis (black).

The phase lag defined above is invariant to shifts of a full period, that is, for a harmonic signal with period of 2 weeks it would not see the difference between 1 week delay and 3 weeks delay. In the theoretical analysis on simple forcing signals in Section 3 it will be shown however that in most cases the delay should be (significantly) shorter than the forcing period. It is assumed that this conclusion carries over to more complex practical cases.

It should be noted that the phase lag defined above is still a measure of *correlation*. Hence, it does not imply causality between the forcing and salinity. Most obviously, the delay can be negative, implying the salinity leads a certain forcing (say, dispersion). Such situation can be found if there are multiple forcing signals and salinity responds dominantly to another forcing (say, discharge). However, also a positive delay does not automatically imply a causal relation, and one should remain careful in the interpretation of the results (see more on this in Section 4).

Simplification in case of harmonic forcing: due to the nature of the of the Morlet wavelet, the wavelet transform (i.e., CWT) of a periodic signal is identical to the Fourier transform. The phase difference obtained from a WCT is therefore also identical to the phase difference one would obtain from a Fourier transform. This is verified for the results in this study in SI-2 (Figures S1–S4 in Supporting Information S1). Hence, in the case of periodic forcing, the definition of delay time simplifies. Thus using the notation in terms of Fourier components in 6a–6c and 10, the delay time for harmonic signals is rewritten as

$$T_{\text{delay}}\left(T_{\text{forcing}}\right) = \begin{cases} \dfrac{\phi[\hat{s}_1] - \phi\left[\hat{K}_{h,1}\right]}{2\pi} T_{\text{forcing}}, & \text{for periodic } K_h, \\ \dfrac{\phi[\hat{s}_1] - \phi[\hat{s}_{\text{sea},1}]}{2\pi} T_{\text{forcing}}, & \text{for periodic } s_{\text{sea}}, \\ \dfrac{\phi[\hat{s}_1] - \phi\left[\hat{Q}_1\right] + \pi}{2\pi} T_{\text{forcing}} & \text{for periodic } Q, \end{cases} \tag{12}$$

where $\phi[\cdot]$ denotes the angle of a complex number.

Adjustment timescale: whereas the delay time represents an actually observed delay, the adjustment time scale $T_{\text{adj},0}$ defined in Equation 4 is only a typical time scale. Nevertheless, as $T_{\text{adj},0}$ provides a useful intuitive and easy time scale, throughout this work I will compare $T_{\text{adj},0}$ to T_{delay}. To this end, the definitions of Q_0 and $K_{h,0}$ used for $T_{\text{adj},0}$ need to be made more precise. For general forcing signals, I will define Q_0 and $K_{h,0}$ as a Gaussian average of $Q(t)$ and $K_h(t)$ over a time window with typical length T_{forcing}, that is,

$$Q_0\left(t, T_{\text{forcing}}\right) = \frac{1}{\sqrt{2\pi}} \int_{-\infty}^{\infty} Q\left(t'\right) e^{-\frac{1}{2}\left(\frac{t'-t}{T_{\text{forcing}}}\right)^2} dt',$$

$$K_{h,0}\left(t, T_{\text{forcing}}\right) = \frac{1}{\sqrt{2\pi}} \int_{-\infty}^{\infty} K_h\left(t'\right) e^{-\frac{1}{2}\left(\frac{t'-t}{T_{\text{forcing}}}\right)^2} dt'.$$

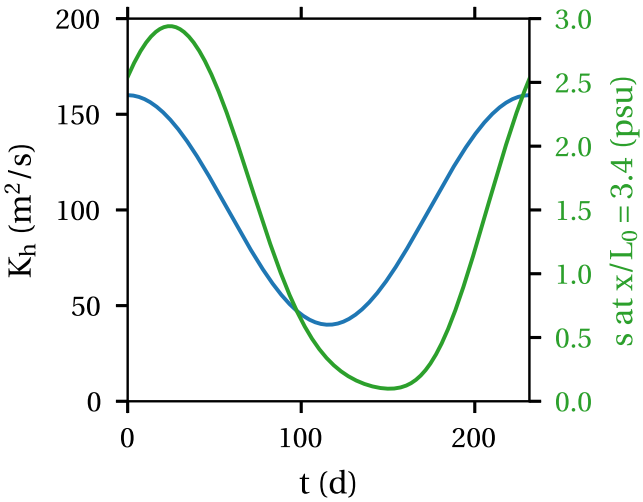

Figure 2. Illustration of the salinity (green, right axis) at a fixed location ($x = 34$ km) under harmonic variation of K_h (blue, left axis) with constant discharge and seaward salinity.

This definition ensures that Q_0 and $K_{h,0}$ represent the actual background conditions as they vary over time, yet this background varies gradually with respect to the forcing time scale that is investigated.

3. Results

The dependence of the delay time on the model variables is investigated for the various types of forcing. First, Section 3.1 illustrates the salinity and delay for a single example. Next, Sections 3.2 and 3.3 discuss results for small-amplitude and general amplitude harmonic forcing. Finally, Section 3.4 shows the behavior of the delay time for peak forcing signals.

3.1. Illustration of a Model Result

I first illustrate a model result for a case with $A = 1 \cdot 10^4$ m^2, $s_{sea} = 30$ psu, $Q = 100$ m^3/s, and $K_h = 100 + 60\cos\left(\frac{\pi t}{T}\right)$ with $T = 230$ days. Figure 2 shows the diffusivity and salinity at $x = 34$ km, which corresponds to $\frac{x}{L_0} = 3.4$, which is the position of the 1 psu line in the case the forcing would not vary in time. The salinity (green line) varies with the diffusivity but with a delay: the maximum salinity is attained 23 days after the maximum diffusivity, while the minimum salinity is attained 36 days after the minimum diffusivity. In the remainder of this study, the delay is measured as defined in Section 2.5 based on the WCT phase. Using this method, $T_{delay} = 26$ days, representing an average delay over the entire period. As a periodic signal is considered here, this is equivalent to the phase difference between the Fourier components with period 230 days. This example clearly shows that other definitions of delay, for example, based on minimum or maximum salinity, may show different delays with respect to the forcing than the definition employed here.

3.2. Small-Amplitude Harmonic Forcing

Next, I will focus on small-amplitude harmonic forcing variations. Looking closer at the analytical solution for the salinity for small-amplitude harmonic forcing in Equation 9, it is found that the delay between the salinity and forcing only depends on two parameters: $\frac{T_{forcing}}{T_{adj,0}}$ and $\frac{x}{L_0}$. For the results, therefore, these two dimensionless parameters will be varied instead of setting values for the dimensional parameters. As long as the amplitude of the forcing variations are small, the forcing amplitude only affects the magnitude of the salinity variations, not the delay. Furthermore, the delay time between salinity and Q or K_h have the same dependency on the two parameters mentioned above, while the delay between salinity and s_{sea} behaves differently.

First I focus on the delay between salinity and K_h or Q. Figure 3 shows the delay time relative to $T_{adj,0}$ (panel a) and relative to $T_{forcing}$ (panel b) as a function of $\frac{T_{forcing}}{T_{adj,0}}$ and $\frac{x}{L_0}$. Shown are results for values of $\frac{x}{L_0}$ that correspond to the average location of the 1, 2, 10, and 20 psu isohalines. The dashed line in both panels indicates a delay of 25% of the forcing period, equivalent to a phase difference of 90°. If the forcing varies rapidly compared to the

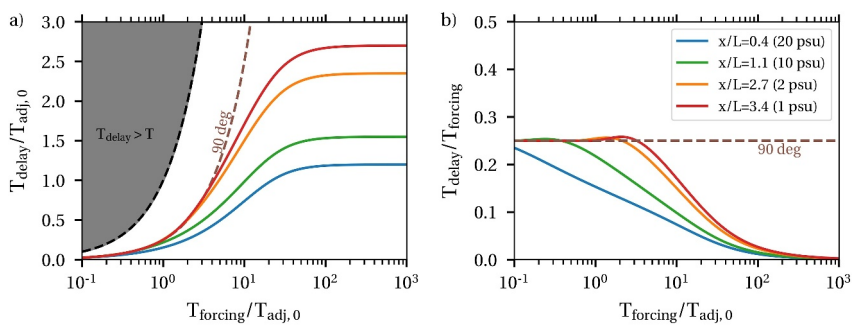

Figure 3. The delay time for small-amplitude harmonic variations in Q or K_h along various isohalines plotted in two ways: normalized by $T_{adj,0}$ (a) and $T_{forcing}$ (b). Delay is plotted as a function of $\frac{T_{forcing}}{T_{adj,0}}$ and the along-channel position in the estuary.

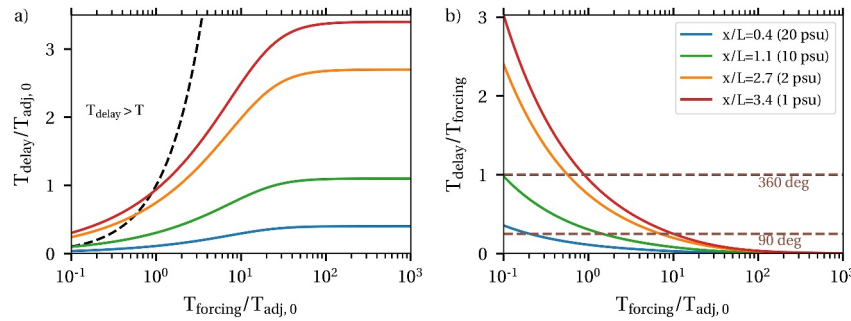

Figure 4. As Figure 3 but for small-amplitude harmonic variations in s_{sea}.

adjustment time (i.e., $\frac{T_{forcing}}{T_{adj,0}}$ small), the observed delay time is approximately 25% of the forcing period (panel b) and hence much smaller than the adjustment time (panel a). This is consistent with earlier findings of Hetland and Geyer (2004). If the forcing varies slowly compared to the adjustment time (i.e., $\frac{T_{forcing}}{T_{adj,0}}$ large), the observed delay is proportional to the adjustment time (panel a).

Interestingly, and not identified earlier in literature, the constant of proportionality between T_{delay} and $T_{adj,0}$ depends on the position along the estuary. Locations further upstream in the estuary show a larger delay time. Using the analytical solution 9, the dependency of the delay time on the along-channel location in the limit for very slow forcing variations is found to satisfy

$$\lim_{\frac{T_{forcing}}{T_{adj,0}} \to \infty} T_{delay} = T_{adj,0}\left(1 + \frac{1}{2}\frac{x}{L_0}\right). \tag{13}$$

Hence, close to the mouth the delay is approximately equal to the adjustment time, while it is a factor 2.7 larger than the adjustment time at the 1 psu isohaline $\left(\frac{x}{L_0} = 3.4\right)$. A technical detail: at $x = 0$ the delay between s and Q or K_h is still formally defined, even though the modeled salinity equals s_{sea} and is independent of Q and K_h.

For intermediate values of $\frac{T_{forcing}}{T_{adj,0}}$ in Figure 3, the delay shows a smooth transition between both extremes. Looking at the results for the 1 or 2 psu isohaline, the figure shows that the delay time is still close to 25% of the forcing period even if the forcing period is already five times larger than the adjustment time. The asymptotic result for slowly varying forcing in Equation 13 is only attained if the forcing period is approximately a factor 100 larger than the adjustment time.

Next, the delay time between the salinity and s_{sea} is shown in Figure 4. If the forcing by s_{sea} varies rapidly compared to the adjustment time (i.e., $\frac{T_{forcing}}{T_{adj,0}}$ small) the observed delay is not restricted by the period of the forcing signal. As seen in panel b, near the 1 or 2 psu isohaline, the delay is even much more than one forcing period (i.e., >360 deg). Analysis of the analytical solution 9 shows that the delay time scales linearly with $\frac{x}{L_0}$. The variation in s_{sea} thus propagates like a wave upstream. As $\frac{T_{forcing}}{T_{adj,0}}$ increases, the propagation speed decreases. Correspondingly, the delay time increases. For $\frac{T_{forcing}}{T_{adj,0}}$ large, the delay time finally converges to

$$\lim_{\frac{T_{forcing}}{T_{adj,0}} \to \infty} T_{delay} = T_{adj,0}\frac{x}{L_0}. \tag{14}$$

Clearly, the delay of salinity to changes in s_{sea} behaves differently to the delay to changes in Q or K_h. In reality, variations in Q, K_h, and s_{sea} are coupled. Due to the differences in response to both forcing parameters, the delay time resulting from this interaction is not trivial. This interaction depends on the estuary and the geometry of the adjacent sea or ocean and is not further explored in this study.

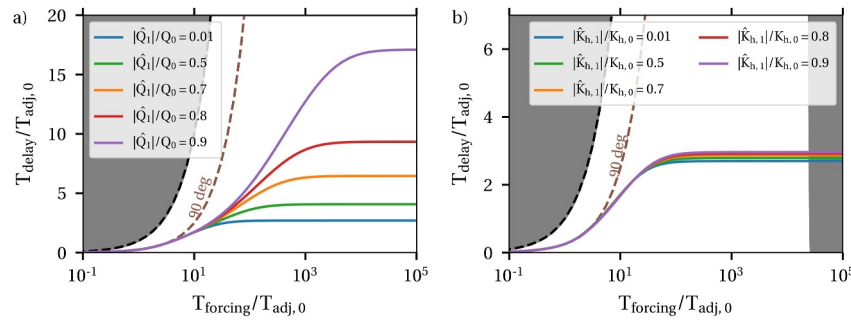

Figure 5. Delay normalized by $T_{adj,0}$ for general amplitude harmonic variations in Q (a) and K_h (b) at a fixed location $\frac{x}{L_0} = 3.4$.

3.3. General-Amplitude Harmonic Forcing

In this section, the amplitude of the harmonic oscillations is arbitrary. Hence, the delay time of the salinity with respect to the forcing parameters depends not only on $\frac{T_{forcing}}{T_{adj,0}}$ and $\frac{x}{L_0}$ but also potentially on the forcing amplitudes $\frac{|\hat{Q}_1|}{Q_0}$, $\frac{|\hat{K}_{h,1}|}{K_{h,0}}$, and $\frac{|\hat{s}_{sea,1}|}{s_{sea,0}}$. In the model experiments in this section, the relative distance $\frac{x}{L_0}$ is fixed at 3.4, which corresponds to the position of the 1 psu isohaline if the forcing were constant in time. For large-amplitude forcing variations, the salt intrusion length will be larger on average (see also Monismith, 2017) and hence $\frac{x}{L_0} = 3.4$ corresponds to a higher average salinity than 1 psu.

Figure 5 shows the delay time relative to the adjustment time as a function of $\frac{T_{forcing}}{T_{adj,0}}$ and the forcing amplitude for variations in Q (panel a) and K_h (panel b). Focusing first on panel a, for small variations in the amplitude of Q, the results are retrieved as in the previous section. As long as the forcing period is not too large compared to the adjustment time, that is, $\frac{T_{forcing}}{T_{adj,0}} < 20$, the amplitude of discharge variations has almost no effect on the delay time. In such cases, the salinity cannot fully adapt to the varying discharge. The salinity profile will therefore look like the salinity profile for constant Q_0 plus a relatively small temporal variation. Consequently, the results are similar to the small-amplitude case considered in Section 3.2. Only if the forcing period is much larger than the adjustment time $\left(\frac{T_{forcing}}{T_{adj,0}} > 100\right)$ is the delay time dependent on the amplitude of discharge variations. In such cases, the salinity does adapt to the varying discharge.

To explain this, consider the following reasoning. The average delay over the forcing period is the result of the adaptation of the salinity at each time instance. Assuming $T_{forcing}$ is large, we are approximately in quasi-equilibrium and at each time instance the adjustment time scales with $\frac{A^2 K_{h,0}}{Q_0^2}$ (see Equation 4). Due to the inverse square relation between this adjustment time and discharge, the overall delay over the entire period is dominated by the slow adjustment at times with low discharges. Hence, the delay is larger when the amplitude of discharge variations is large.

The amplitude of variations of K_h (panel b) has an almost negligible influence on the delay time. Using a similar reasoning as above, assuming a quasi-stationary state, the salinity adjusts with a time scale $\frac{A^2 K_{h,0}}{Q_0^2}$. While this means the response is slow when $K_h(t)$ is large and vice versa, these difference cancel out when averaged, and the delay almost only depends on the average value of $K_h(t)$.

The amplitude variations of s_{sea} do not affect the delay time in this model. Hence, Figure 4 applies regardless of the amplitude of s_{sea} variations.

3.4. Peak Forcing

Next considered are peak forcing signals. To this end, I compute the salinity over 1 year (i.e. $T = 365$ days), with constant forcing apart from one peak that reaches its maximum at $\frac{1}{2}T$. The peak is chosen to take the shape of only the positive part of a sine wave with various values for the peak amplitude and duration (see Figure 6a for an example). Below, I only present results for peak forcing in discharge. The results for peak forcing in K_h and s_{sea}

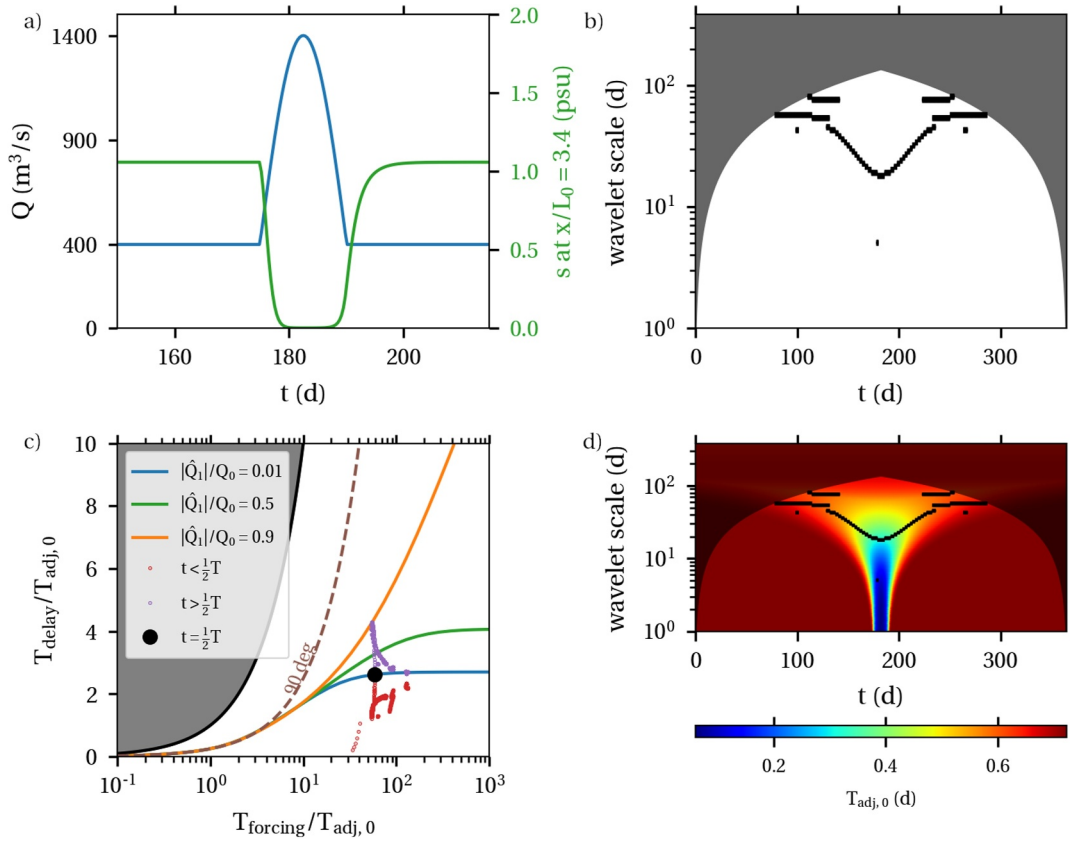

Figure 6. Results for a discharge peak forcing experiment. (a) Discharge signal (blue) and resulting salinity at $\frac{x}{L_0} = 3.4$ (green). (b) Points in the (t, T_{forcing})-space where the time delay is considered (black dots) and the cone-of-influence, where results cannot be used due to the endpoints of the time series. (c) Delay time versus forcing time, scaled by $T_{\text{adj},0}$ at $\frac{x}{L_0} = 3.4$. Dots indicate the delay before, at, and after the maximum discharge is attained. The lines indicate the results obtained earlier using harmonic forcing. (d) $T_{\text{adj},0}$ as a function of t and T_{forcing}. Black markings as in panel (b).

result in delay times that are very similar to the results when using periodic forcing, as demonstrated in SI-3 (Figure S5 in Supporting Information S1). An example of a peak forcing in discharge is shown in Figure 6 with a peak duration of 15 days (period of full sine wave is 30 days) and amplitude of 1,000 m^3/s. Figure 6a shows the discharge and resulting salinity at $x = 3.4L_0$. The salinity responds asymmetrically: it adjusts faster to increasing discharge than to decreasing discharge similar to the periodic case illustrated in Figure 2, see Chen (2015) for an extensive discussion. Figure 6b shows a (t, T_{forcing})-diagram. The shaded area is the cone-of-influence, where the results of the wavelet analysis are not reliable due to the effects of using a finite time series. The black markings indicate the points where the WCT phase difference is considered, based on the selection criteria presented in Section 2.5 (i.e., significance and maximum amplitude in T_{forcing}). These points have a wavelet scale (vertical axis) that varies between 18 and 75 days over time. It is interesting to note that the sine-wave used as input for Q has a period of 30 days, but the wavelet analysis does not uniformly identify this period. The analysis already yields results around the 50 and 75 days wavelet scale for $t < 100$ days, while the discharge peak only starts on day 170. This is because the wavelet analysis operates on a Gaussian window that scales with the wavelet scale. The window centered around, for example, $t = 100$ days at wavelet scale 50 days extends over day 170 and hence registers a signal. This can be interpreted as some measure of the delay when only considering the start of the discharge peak. Similarly, the wavelet signal extends until well after day 250, when the salinity has already returned to its equilibrium value. As Q_0 is not constant in this model experiment, $T_{\text{adj},0}$ is not a constant and Figure 6d shows the adjustment time $T_{\text{adj},0}$ as a function of time and wavelet period. The black markings are the same as in panel b and we see that at these markings, $T_{\text{adj},0}$ varies between 0.3 and 0.6 days. Figure 6c shows the delay time against the forcing time, both scaled by $T_{\text{adj},0}$. The colored lines indicate the results found earlier for periodic signals at $\frac{x}{L_0|_{t=0}} = 3.4$ (c.f. Figure 5). The dots show the delay time computed from the WCT phase

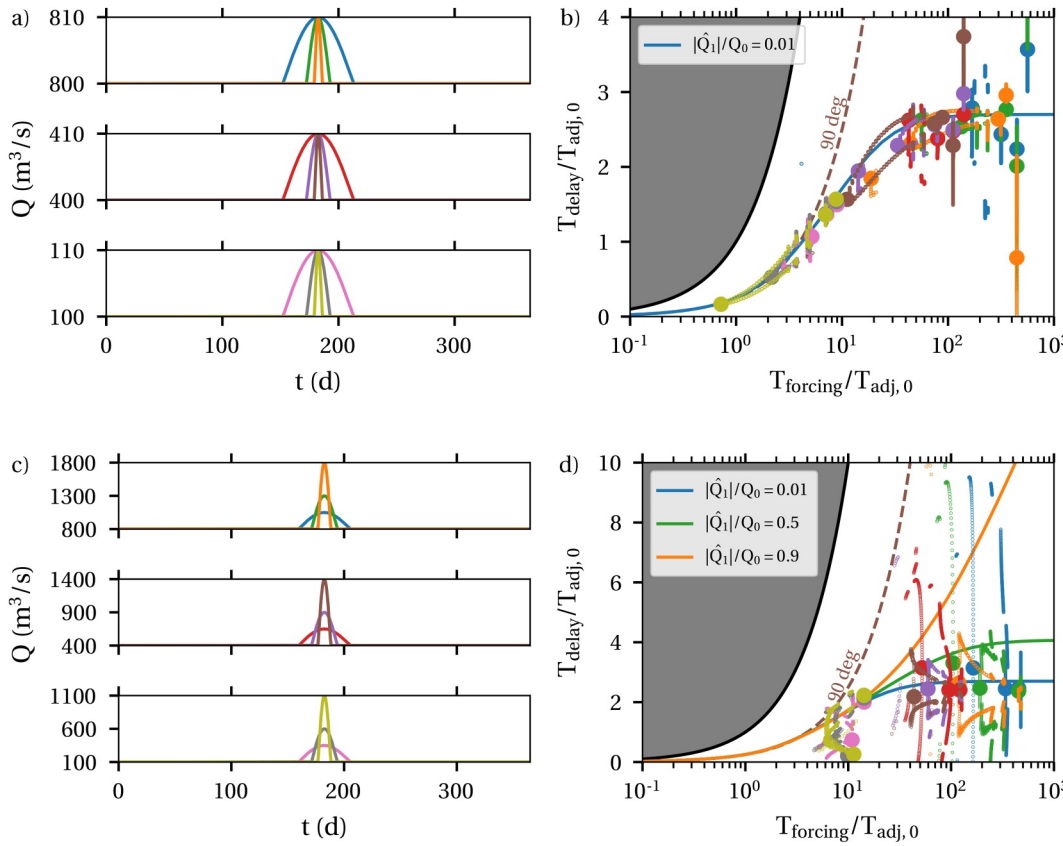

Figure 7. Various peak signals with small amplitude (a) and large amplitude (c) and the delay time resulting from the wavelet analysis (b), (d) in matching colors. The large dots represent the delay at $t = \frac{1}{2}T$, where the discharge attains its maximum. Note that multiple large dots in one color can appear, as the wavelet analysis identifies several significant timescales at $t = \frac{1}{2}T$. Smaller dots correspond to the delay measured at other times.

difference. Red and purple dots indicate the delay at times before and after the maximum discharge is reached, respectively.

Figure 6c shows that the wavelet analysis identifies a variation in the typical timescale of the forcing and delay over the course of the peak forcing. The delay is smaller than average before the maximum discharge is reached and larger than average after the maximum discharge is reached. This corresponds to the observed asymmetry in s (panel a) and Chen (2015). There are a few red points that indicate a small delay $\left(\frac{T_{\text{delay}}}{T_{\text{adj},0}} < 1\right)$, which correspond to the outliers in the (t, T_{forcing})-diagram (Figure 6b) with wavelet timescale of 5 days and are probably spurious.

The red and purple dots meet at $t = \frac{1}{2}T$ (black circle) with $\frac{T_{\text{delay}}}{T_{\text{adj},0}} \approx 2.5$ and $T_{\text{adj},0} \approx 0.28$ days (with wavelet scale of 18 days). Hence $T_{\text{delay}} \approx 2.5 \times 0.28 \approx 0.7$ days. Comparing the black circle to results for harmonic forcing (solid lines), the value of $\frac{T_{\text{delay}}}{T_{\text{adj},0}}$ is close to the result for small-amplitude periodic waves. This may be surprising as the peak forcing has a very large amplitude. To explain this, consider a simple harmonic forcing that resembles the peak forcing close to the peak. This harmonic signal would have a mean discharge of about 900 m^3/s and amplitude of about 500 m^3/s. As $\frac{|\hat{Q}_1|}{Q_0} \approx 0.5$, this harmonic signal would have a $\frac{T_{\text{delay}}}{T_{\text{adj},0}} \approx 4.5$ (green line in Figure 6c), and $T_{\text{adj},0}$ would be approximately equal to 0.14 days (Figure 6d). The delay of such harmonic signal would therefore be $T_{\text{delay}} = 4.5 \times 0.14 = 0.6$ days, which is not too far from the 0.7 days delay of the peak forcing computed for $t = \frac{1}{2}T$.

Figure 7 shows the delay in response to various peak discharges. The upper row focusses on small-amplitude peaks with various durations. Figure 7a shows the discharge and Figure 7b shows the delay using matching

colors. The delay generally follows the results obtained with small-amplitude harmonic forcing (blue line) with some asymmetry in the delay for increasing and decreasing discharge. For large forcing period, deviations occur showing some very small or large values of $\frac{T_{\text{delay}}}{T_{\text{adj},0}}$, which I expect to be spurious. Overall however, the conclusions drawn for small-amplitude harmonic forcing carry over to small-amplitude peak forcing. Figures 7c and 7d follow a similar format for large-amplitude forcing. The resulting delay has most points varying around the line for small-amplitude harmonic forcing, as we have seen in Figure 6. However, the wavelet analysis also shows an extensive range of very large and small delay times. The small delay times correspond to times with increasing discharge, while the large delay times correspond to times with decreasing discharge. This is consistent with results found earlier in Figure 6, but this effect seems much more pronounced. Nevertheless, even the largest reported delay times roughly remain smaller than 25% of the forcing period. The delay for small-amplitude harmonic forcing seems to be a good indication of a typical delay time for large-amplitude peak forcing as well, although the wavelet analysis registers a significant variation about this.

4. Discussion

The results discussed above are for quite theoretical forcing signals and a simple linear model. While this sets a clear theoretical framework, in this section I will discuss to what extent these theoretical results can be recognized in some more complex and realistic situations. First, in Section 4.1 I present the delay within the same linear model but for realistic and simultaneously varying Q and K_h inspired from observations. Next, in Section 4.2, I discuss how these results generalize to non-linear salinity models, including a discussion of some of the limitations of this work.

4.1. Delay for Realistically Varying Parameters

This section illustrates the application of the wavelet analysis and computation of delay for a more realistic setting, with realistically and simultaneously varying Q and K_h. This case is inspired by the Modaomen estuary (China) as presented by Payo-Payo et al. (2022) (*hereafter* PP22). They simulated the salinity using a 3D model in FVCOM over a 9-month period that includes the transition from dry to wet season. The model included a fully realistic set-up of the entire Pearl River Delta and coastal zone, forced by observed winds, tides and discharge and solving the hydrostatic equations of motion, salinity equation and a $k-\epsilon$ turbulence closure model. To restrict complexity, I apply the linear salt model 2 with constant cross-sectional area with parameters representative for the Modaomen estuary. The varying discharge is directly used from PP22 and shown in Figure 8a. The seaward salinity is assumed constant for simplicity at a location 5 km downstream of the south-section in PP22. While this does not fully match the 3D model results, this assumptions suffices for the illustrative purposes of this study. The time-dependent K_h is chosen such that the 0.5 psu line in the linear model matches the tidally averaged near-bed 0.5 psu line in the 3D model of PP22 at every moment in time. Hence, K_h parametrizes the total dispersion following from the 3D model. The resulting signal for K_h is shown in Figure 8b and shows a clear spring-neap variation as well as a seasonal variation. The salinity at a fixed location $x_1 = 5$ km (i.e., the location of the south section in PP22) resulting from the linear 1D model is plotted in Figure 8a (green line). The delay is computed at the same location and analyzed below.

Figures 8c and 8d show the adjustment time $T_{\text{adj},0}$ (color scale; same in both panels). The adjustment time varies between 0.1 day and 2.5 days. On the shorter wavelet periods, the adjustment time shows a clear spring-neap variability as the dispersion parameter varies over the spring neap cycle. On a bigger time scale, there is a clear seasonal difference, with the transition between the dry and wet season around $t = 180$ days. Related to the change in discharge, the adjustment time drops from roughly 1.5–2.5 days to 0.1–0.5 days around this seasonal transition. The black markings in the figure indicate the relevant points in the time-wavelet period space identified using the criteria from Section 2.5 for Q (Figure 8c) and K_h (Figure 8d). These points are on various wavelet periods in both Q and K_h. This qualitatively matches PP22, who also identified a wide variety of relevant wavelet periods. Notably, a 14 days scale is observed in K_h, matching the spring-neap cycle.

Figure 8e shows the delay time plotted against forcing time, both normalized by the adjustment time, with respect to discharge. It shows quite a few points near the theoretical line for small-amplitude harmonic forcing (blue line), but also a large scatter. This is not unlike the results for large-amplitude peak forcing (c.f. Figure 7d) but with a larger extent of the variations. These results are not surprising as the forcing signal of the discharge is much more complex and looks like a sequence of peaks.With the single peaks in Section 3.4, a clear structure could be

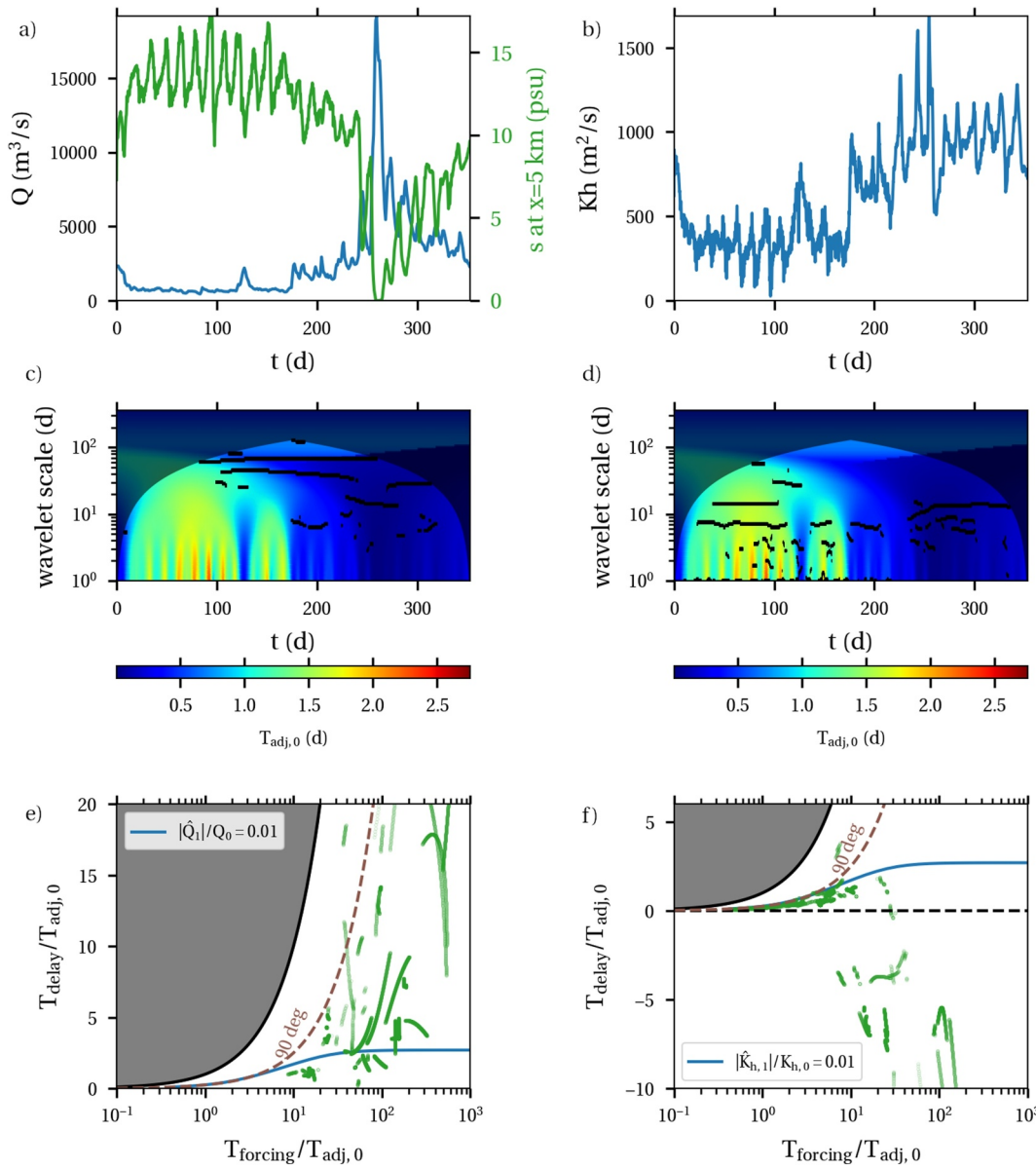

Figure 8. Realistic forcing signals for Q, K_h based on PP22 for the Modaomen and salinity from the linear 1D model at $x = 5$ km (panels (a), (b)). Panels (c), (d) show $T_{adj,0}$ as a function of time and forcing time scale (colors) as well as the points were the delay is considered (black dots) for the forcing by discharge (c) and dispersion parameter (d), respectively. Panels (e), (f) show the delay time as function of the forcing time scale, scaled by $T_{adj,0}$ with respect to the forcing by discharge (e) and dispersion parameter (f). The blue line indicates the result for small-amplitude harmonic forcing, as reference. The brown dashed line indicates a delay of 25% of the forcing time.

identified, with longer delay after the peak and shorter delay before the peak. I was not able to identify this structure from the signal in this case, as peaks follow one another rapidly and the salinity is hence always adjusting to multiple peaks in discharge simultaneously. The main conclusion that can be drawn is hence that most delay times remain below 25% of the forcing time scale. Also a significant number of points is quite close to the results for harmonic forcing (blue line).

The delay with respect to K_h (Figure 8f) shows two quite different aspects. For small $\frac{T_{delay}}{T_{adj,0}}$ (roughly <10), results follow the delay for small-amplitude harmonic signals. These results correspond mostly to $t < 180$ days, when the discharge is fairly constant and K_h and salinity both vary dominantly on a spring-neap scale. Hence, the setting is reasonably close to the harmonic setting, which is also reflected in quite regular results. For larger relative forcing

period, the delay is negative. These negative delay times indicate a non-causal relationship. Since the salinity is affected by variations in both Q and K_h, the salinity is not only caused by either Q or K_h but by both. Causal relations between salinity and only one forcing variable is only reasonable to assume if the forcings act on clearly different timescales or the considered forcing is dominant. Analysis shows that the negative delays correspond to $t > 180$ days, where the variations in Q and K_h are on very similar timescales and the variations in Q are quite large. Hence, it is reasonable that the salinity does not have a clear causal relation to K_h considered in isolation. This limitation is important to consider in realistic application of the wavelet analysis, because salinity is usually driven by more than one varying forcing (e.g., tide, discharge, wind).

Main lessons for general applicability: Reflecting on the results, on the one hand there are important parts of the theory that stand out. Most importantly, assuming causality, delay is less than 25% of the forcing period. For small relative forcing period (i.e., <5 to 10 times $T_{\text{adj},0}$), the delay is quite close to this 25%, so the delay with respect to forcing variations on each timescale can be estimated well. The scatter found for delay w.r.t. Q is also quite typical for peak-like forcing. However, it is now found that scatter is not only larger due to the complexity of the signals, but also that scatter cannot be as well interpreted as in individual peaks. Also causality is no longer guaranteed since now two (partly interdependent) forcing processes are considered.

The definition of delay per timescale in this work considers the delay between two general signals without necessarily requiring any model, assumptions, processing or filtering beforehand. It is thus only logical that an input of non-causal signals or highly complex signals yields delays that are quite hard to interpret or carry no physical meaning. The illustration here clearly demonstrates this. Further improvements in the interpretation of realistic signals likely require better theoretical understanding as suggested in Section 4.3.

4.2. Generalization to Nonlinear Salinity Models and Nonuniform Geometry

In general, salt transport follows strongly nonlinear laws due to the effects of salinity on density. A general 1-dimensional salt model can be written as

$$As_t = (Qs + D(x,s,s_x))_x, \tag{15}$$

where D is some function of x, s, and s_x. Such general 1-dimensional form can represent the salinity in many well-mixed and partially stratified estuaries. It thus provides sufficient possibilities to parametrize the effects of averaging over the cross-section and the tidal time scale (see e.g. Fischer et al., 1979; Savenije, 2012, for reviews). This nonlinear equation may be approximated by our linear equation when considering small variations. To this end, assume the salinity has the form $s(x,t) = \bar{s}(x,t) + s'(x,t)$, where $\bar{s}$ is some known slowly varying background state and s' is a small variation. The linearized equation for s' then reads as

$$As'_t = \left(\left(Q + \frac{\partial D}{\partial s}\right)s' + \frac{\partial D}{\partial s_x}s'_x\right)_x.$$

This has the same form as Equation 2 with $Q + \frac{\partial D}{\partial s}$ replacing the discharge and $\frac{\partial D}{\partial s_x}$ replacing the dispersion parameter. Hence, our results may be used directly for analyzing small variations of the salinity around some slowly varying background state. As long as forcing signals have a time scale that is not too large compared to the adjustment time, for example, $\frac{T_{\text{forcing}}}{T_{\text{adj},0}} < 10$, the salinity can only partially adjust to the changing forcing. The salinity in that case is always a small variation about a slowly varying background state. Hence, the conclusions drawn in this study for $\frac{T_{\text{forcing}}}{T_{\text{adj},0}} < 10$ also apply approximately to nonlinear models.

Quite commonly, the form of D is restricted to a form $C_1 s_x^n + C_2 s^m$ for constants C_1, C_2, n, and m (see e.g. Savenije, 2012). For example, in estuaries strongly controlled by density-driven flow, D scales with s_x^3 (see e.g. MacCready, 2004). For such forms of D, the linear model may also be used as a post-processing tool for large variations in salinity. In this case, the salt model 15 is rewritten to

$$As_t = \left(\left(Q + C_2 s^{m-1}\right)s + C_1 s_x^{n-1} s_x\right)_x \tag{16}$$

and $Q + C_2 s^{m-1}$ thus replaces the discharge and $C_1 s_x^{n-1}$ replaces the dispersion parameter. In post-processing, s is known, so $Q + C_2 s^{m-1}$ and $C_1 s_x^{n-1}$ are known. The non-linearity then translates into a known time-variation of the discharge and dispersion parameter. The main conclusions from this study therefore also apply for any forcing condition when using a nonlinear salinity model with the imposed form of D.

4.3. Suggestions for Further Theoretical Extension

In a realistic setting of a stratified estuary, dispersion and seaward salinity are not simply external parameters, but depend on the salinity itself. Hence, a variation in discharge can cause a change in the dispersion and seaward salinity with a certain delay, which itself creates a new delayed response in salinity. It is useful to further explore the effect of such nonlinear relations within the context of the theory developed here, so as to better understand observations in real estuaries. MacCready (2007) already showed that the adjustment time for partially stratified estuaries, accounting for this nonlinear coupling, is clearly different from the linear case that better represents well-mixed estuaries. This also implies that adjustment time and therefore likely delay time is a function of the estuarine regime.

Results in this work were all done assuming all parameters are along-channel uniform. The results remain valid when varying the parameters along the channel, however it becomes unclear how to define the adjustment time $T_{\mathrm{adj},0}$. This does not only depend on the parameters at one cross-section but on the parameters in the entire estuary. More work is needed to find an appropriate definition for $T_{\mathrm{adj},0}$ in this case.

Finally, it was here assumed that s_{sea} variations can simply be imposed, while in reality this still depends on interaction with the sea or ocean. Also, the effect of varying s_{sea} has not been tested in a more realistic context. In the theoretical cases, the delay w.r.t. s_{sea} could be larger than the forcing period. Since the delay from wavelet analysis cannot distinguish delays that are exactly a forcing period apart, it is questionable whether the large delays appearing in simple cases can be identified in more complex signals. Also, since there are potentially strong relations between discharge, dispersion and s_{sea} in a realistic context, it is unclear whether delays w.r.t. s_{sea} offer any clear interpretation.

5. Conclusions

The delayed response of salinity to changes in discharge and dispersion were investigated. The delay was measured using a phase difference in the wavelet coherence. This method allows computation of delays w.r.t. forcing variations on various timescales between any forcing signal and salinity, whether modeled or measured. The method therefore clearly extends the possibilities beyond some other definitions that only applied to highly idealized cases. While measures for delay based on windowed Fourier transforms or wavelet analysis have been used before (e.g., PP22), to the author's knowledge this is the first time this measure is strictly defined, including a set of rules on relevant points in the wavelet space where this delay should be evaluated, hence automating the calculation process.

The main new insights into delay have been obtained by applying it to simple forcing signals. When considering harmonic forcing in the forcing, clear one-to-one relations were found between delay and the duration and amplitude of the forcing. For forcing signals consisting of a single peak, results were not one-to-one, but still revealed quite similar relations. The following results were identified in the context of these simple forcing signals.

1. The delay depends on the timescale T_{forcing} (e.g., period/duration) of a forcing variation, relative to the adjustment time $T_{\mathrm{adj},0}$. Here the adjustment time only depends on the background conditions of the estuary. When approximately $T_{\mathrm{forcing}} < 5T_{\mathrm{adj},0}$, the delay is around 25% of the forcing timescale. For very large T_{forcing} (i.e., $T_{\mathrm{forcing}} > 100T_{\mathrm{adj},0}$), the delay is proportional to $T_{\mathrm{adj},0}$. For all intermediate forcing timescales, the delay time varies as a function of T_{forcing} and $T_{\mathrm{adj},0}$. In practice this means that the observed delay in salinity cannot simply be explained by $T_{\mathrm{adj},0}$, but should account for T_{forcing} as well.
2. The delay time depends the location along the estuary, where locations further upstream experience significantly larger delays between forcing and salinity.
3. The delay with respect to discharge variations depends on the magnitude of the forcing variation, where occurrences of low discharges cause disproportional increases in the delay time. In the wavelet analysis, this is identified as a large scatter in delay time, locally peaking to high values.

Although results were obtained with a simple linear model in a straight uniform estuary, it was reasoned that the main conclusions apply qualitatively for much more general nonlinear salinity models and non-uniform geometries.

Data Availability Statement

The model is available under iFlow version 3.1 on GitHub (iFlow Modelling Framework (Version 3.1), 2024), along with the input file and data needed to run the Modaomen test case.

Acknowledgments
This research was funded by the Dutch Science Organisation (NWO, Grant ALWSD.2016.015).

References

Banas, N. S., Hickey, B. M., MacCready, P., & Newton, J. A. (2004). Dynamics of Willapa Bay, Washington: A highly unsteady, partially mixed estuary. *Journal of Physical Oceanography*, *34*(11), 2413–2427. https://doi.org/10.1175/jpo2637.1

Biemond, B., de Swart, H. E., Dijkstra, H. A., & Díez-Minguito, M. (2022). Estuarine salinity response to freshwater pulses. *Journal of Geophysical Research: Oceans*, *127*(11). https://doi.org/10.1029/2022jc018669

Bowen, M. M., & Geyer, W. R. (2003). Salt transport and the time-dependent salt balance of a partially stratified estuary. *Journal of Geophysical Research*, *108*(C5), 3158. https://doi.org/10.1029/2001jc001231

Chen, S.-N. (2015). Asymmetric estuarine responses to changes in river forcing: A consequence of nonlinear salt flux. *Journal of Physical Oceanography*, *45*(11), 2836–2847. https://doi.org/10.1175/jpo-d-15-0085.1

Fischer, H. B., List, E. J., Koh, R. C. Y., & Imberger, J. (1979). *Mixing in inland and coastal waters*. Academic Press.

Gong, W., & Shen, J. (2011). The response of salt intrusion to changes in river discharge and tidal mixing during the dry season in the modaomen estuary, China. *Continental Shelf Research*, *31*(7–8), 769–788. https://doi.org/10.1016/j.csr.2011.01.011

Grinsted, A., Moore, J. C., & Jevrejeva, S. (2004). Application of the cross wavelet transform and wavelet coherence to geophysical time series. *Nonlinear Processes in Geophysics*, *11*(5/6), 561–566. https://doi.org/10.5194/npg-11-561-2004

Hetland, R. D., & Geyer, W. R. (2004). An idealized study of the structure of long, partially mixed estuaries. *Journal of Physical Oceanography*, *34*(12), 2677–2691. https://doi.org/10.1175/jpo2646.1

Hoitink, A. J. F., & Jay, D. A. (2016). Tidal river dynamics: Implications for deltas. *Reviews of Geophysics*, *54*(1), 240–272. https://doi.org/10.1002/2015rg000507

iFlow Modelling Framework (Version 3.1). (2024). GitHub/Zenodo [Software]. https://doi.org/10.5281/zenodo.822394

Kranenburg, C. (1986). A time scale for long-term salt intrusion in well-mixed estuaries. *Journal of Physical Oceanography*, *16*(7), 1329–1331. https://doi.org/10.1175/1520-0485(1986)016⟨1329:atsflt⟩2.0.co;2

Lerczak, J. A., Geyer, W. R., & Ralston, D. K. (2009). The temporal response of the length of a partially stratified estuary to changes in river flow and tidal amplitude. *Journal of Physical Oceanography*, *39*(4), 915–933. https://doi.org/10.1175/2008jpo3933.1

MacCready, P. (1999). Estuarine adjustment to changes in river flow and tidal mixing. *Journal of Physical Oceanography*, *29*(4), 708–726. https://doi.org/10.1175/1520-0485(1999)029⟨0708:eatcir⟩2.0.co;2

MacCready, P. (2004). Toward a unified theory of tidally-averaged estuarine salinity structure. *Estuaries*, *27*(4), 561–570. https://doi.org/10.1007/BF02907644

MacCready, P. (2007). Estuarine adjustment. *Journal of Physical Oceanography*, *37*(8), 2133–2145. https://doi.org/10.1175/jpo3082.1

Monismith, S. (2017). An integral model of unsteady salinity intrusion in estuaries. *Journal of Hydraulic Research*, *55*(3), 392–408. https://doi.org/10.1080/00221686.2016.1274682

Payo-Payo, M., Bricheno, L. M., Dijkstra, Y. M., Cheng, W., Gong, W., & Amoudry, L. O. (2022). Multiscale temporal response of salt intrusion to transient river and ocean forcing. *Journal of Geophysical Research: Oceans*, *127*(3). https://doi.org/10.1029/2021jc017523

Savenije, H. H. G. (2012). *Salinity and tides in alluvial estuaries* (Second Completely Revised ed.). Elsevier.

Torrence, C., & Compo, G. P. (1998). A practical guide to wavelet analysis. *Bulletin of the American Meteorological Society*, *79*(1), 61–78. https://doi.org/10.1175/1520-0477(1998)079⟨0061:apgtwa⟩2.0.co;2

Vijith, V., Sundar, D., & Shetye, S. (2009). Time-dependence of salinity in monsoonal estuaries. *Estuarine, Coastal and Shelf Science*, *85*(4), 601–608. https://doi.org/10.1016/j.ecss.2009.10.003